



LAWRENCE  
LIVERMORE  
NATIONAL  
LABORATORY

# Systematic Studies of Light Neutron-Rich Nuclei produced via the Fragmentation of $^{40}\text{Ar}$

E. Kwan, D. J. Morrissey, D. A. Davies, M. Steiner, C. S. Sumithrarachchi, L. Weissman

March 7, 2012

Physical Review C

## **Disclaimer**

---

This document was prepared as an account of work sponsored by an agency of the United States government. Neither the United States government nor Lawrence Livermore National Security, LLC, nor any of their employees makes any warranty, expressed or implied, or assumes any legal liability or responsibility for the accuracy, completeness, or usefulness of any information, apparatus, product, or process disclosed, or represents that its use would not infringe privately owned rights. Reference herein to any specific commercial product, process, or service by trade name, trademark, manufacturer, or otherwise does not necessarily constitute or imply its endorsement, recommendation, or favoring by the United States government or Lawrence Livermore National Security, LLC. The views and opinions of authors expressed herein do not necessarily state or reflect those of the United States government or Lawrence Livermore National Security, LLC, and shall not be used for advertising or product endorsement purposes.

# Systematic Studies of Light Neutron-Rich Nuclei produced via the Fragmentation of $^{40}\text{Ar}$

E. Kwan,<sup>1,2,\*</sup> D. J. Morrissey,<sup>1,3</sup> D. A. Davies,<sup>1,3</sup>

M. Steiner,<sup>1</sup> C. S. Sumithrarachchi,<sup>1,3</sup> and L. Weissman<sup>1</sup>

<sup>1</sup>*National Superconducting Cyclotron Laboratory, East Lansing, Michigan, 48824*

<sup>2</sup>*Department of Physics and Astronomy,*

*Michigan State University, East Lansing, Michigan, 48824*

<sup>3</sup>*Department of Chemistry, Michigan State University, East Lansing, Michigan, 48824*

(Dated: March 2, 2012)

## Abstract

Radioactive isotopes of Beryllium to Phosphorus were produced by projectile fragmentation of a  $^{40}\text{Ar}$  beam with either a Be, Ni, or Ta target at the National Superconducting Cyclotron Laboratory. The fragmentation cross sections, parallel momentum transfers and widths were systematically measured and compared to the empirical parameterization of EPAX and to predictions from internuclear cascade and deep inelastic codes. The predicted distributions for the widths from the internuclear cascade simulations agree to within one standard deviation with the measured results, while the velocities and cross-sections are found to be more consistent with the deep inelastic transfer calculations. A target dependence was found in the reaction cross sections for the neutron-rich nuclei with the largest  $N/Z$  ratio suggesting an enhancement in the fragment yields larger  $N/Z$  targets.

PACS numbers: 24.10.Lx,25.70.-Mn,27.10.+h,27.20.+n,27.30.+t

---

\*Present address: Physics Division, Lawrence Livermore National Laboratory, Livermore, CA 94550 USA

## I. INTRODUCTION

Nuclei far from stability have attracted much interest because they can exhibit unique features compared to those nuclei near  $\beta$ -stability. The location of the limits of stability is also of great importance in the understanding of how the shell structure might change as nuclei become more exotic. Projectile fragmentation has been the preferred method to produce nuclei near and along the neutron drip line due to the short extraction times compared to other production methods [1]. Accurate predictions of the fragment intensities produced by this method are also important from a practical standpoint. An empirical parameterization formula, EPAX, has widely been used to predict the intensities of nuclei produced from the fragmentation process by assuming that the isobaric mass yields are generally exponential [2]. While this formalization is useful, it gives no information about the production mechanism that creates the fragments and many models that can describe characteristics of near stable nuclei well have been known to fail for nuclei far from stability [3]. Unfortunately, there is no method that can directly observe the intermediate stages of the reaction process at present, thus one must rely on reaction models that attempt to reproduce measured observables such as the cross sections, fragment momenta and widths. Systematic investigations into the reaction mechanism are needed especially for very neutron-rich nuclei at intermediate bombarding energies where the production cross sections from projectile fragmentation are not known with a high degree of accuracy and the observation of new nuclei along the unmapped region along the neutron drip line can yield hints of changing shell structure and nucleon stability.

A high degree of accuracy in the predicted cross sections of fragments near stability has been achieved by the empirical parameterizations called EPAX [2]. These parameterizations were developed for reactions where the yields are energy independent (*i.e.* in the regime of “limiting fragmentation”) and do not generally describe products produced from fission or nucleon pickup. Any influence of the target’s neutron-to-proton ratio ( $N/Z$ ) is neglected in the determination of the fragmentation product’s neutron excess. This assumption may be valid at the high-energy limit where the kinetic energy is much greater than the nuclear potential and the de Broglie wavelength of the projectile is much smaller than the average distance between nucleons in the target. At energies near the Coulomb barrier, the target and projectile rapidly equilibrate their  $N/Z$  ratio due to their long interaction

time. Thus, targets with large  $N/Z$  ratios may increase the yields of neutron-rich fragments at intermediate energies due to the re-absorption of nucleons from the participant zone or nucleon-nucleon exchange during the target-projectile collision [4]. The transition point between the high- and low-energy regimes is not well known and more complete studies of fragmentation at the intermediate energy domain are needed to determine the roles of the two reaction mechanisms at these energies.

Many reaction codes have been developed in attempts to describe the reaction mechanism either at relativistic or nonrelativistic energies. At the relativistic and intermediate energy regimes, the nucleon-nucleon collisions have been described in a microscopic framework using internuclear cascade models such as the Monte Carlo codes VEGAS [5] and ISABEL [6], the latter being a generalized VEGAS code for nucleus-nucleus collision. In these models, the authors assume that the projectile and target move along classical trajectories in the center-of-mass frame until the two nuclei collide with each other allowing nucleons to interact. The interacting nucleons or participants undergo a series of time-dependent two-body nucleon-nucleon collisions starting within the region of overlap between the target and projectile until they escape or fall below the binding energy of the nucleus. The sum of all of the interactions creates an excited prefragment, which then undergoes statistical decay to create the final observed nucleus.

On the other hand, in the nonrelativistic energy regime, it is widely accepted that nucleon transfer mechanisms are the dominant scattering processes aside from fusion that lead to the production of radioactive nuclei. The transfer mechanism is expected to subside as the kinetic energy of projectile increases due to the increasing difference between the projectile and target nucleon momenta. The disappearance of the signatures of the transfer mechanism, such as the suppression of the yields of masses heavier than that of the projectile, has been thought to be an indication of the onset of the fragmentation mechanism. It has also been argued that the nuclei tend to be highly excited and the suppression of their yields may be the result of evaporative processes that occur to deexcite the nucleus thus reducing the number of observed heavy nuclei [7]. A Monte Carlo deep-inelastic transfer model DIT was developed by Tassan-Got and Stépan [7] to predict the reaction yields in the intermediate energy regime. In their code, the nucleon-nucleon transfers during the projectile-target interaction are treated in terms of the tunneling probabilities across their respective potential barriers. The relative velocity of the transferred particles/holes is determined by the

excitation of the prefragment. Both the ISABEL and DIT codes were used in the current work to provide the distribution and excitation energies of the prefragments. The resulting prefragments from the codes were then passed through a statistical deexcitation code to determine the final fragment distributions and momenta for comparison with the results from the current work.

In the present work, systematic measurements of the reaction cross sections, momentum widths and momentum transfers of neutron-rich fragments from  $Z = 4$  to 15 produced by the fragmentation of a  $^{40}\text{Ar}$  projectile at the intermediate energy of 120 MeV/nucleon (the energy at the center of the target) with one of three  $N/Z$  targets:  $^9\text{Be}$ ,  $^{nat}\text{Ni}$ , or  $^{181}\text{Ta}$ . Thick targets on the order of 500-1000 mg/cm<sup>2</sup> were used to enhance the yields of the most neutron-rich nuclei near the limits of stability. A discussion of the corrections made to the parallel momentum widths, and velocities due to the energy loss through the targets is described in Section III A. In Sections III C and III B, the fragment's momentum transfers and widths are presented, respectively, and the reaction mechanism is analyzed using an empirical parameterization. Comparisons of the measured reaction cross sections from the current work with a previous measurement and two Monte Carlo codes are presented in Section III D.

## II. EXPERIMENTAL SETUP

Light neutron-rich nuclei were produced at the National Superconducting Cyclotron Laboratory (NSCL) by projectile fragmentation of a  $^{40}\text{Ar}$  beam accelerated to 140 MeV/nucleon by the coupled cyclotrons on one of three targets, a 668 mg/cm<sup>2</sup>  $^9\text{Be}$ , 775 mg/cm<sup>2</sup>  $^{nat}\text{Ni}$ , and 1086 mg/cm<sup>2</sup>  $^{181}\text{Ta}$ , in order to study the affect of the neutron excess of the target on the production yields of nuclei near the neutron drip line. The target thicknesses, chosen on the basis of the energy losses of the  $^{40}\text{Ar}^{18+}$  in the targets, were chosen to maximize the production of those nuclei near the neutron drip line while yielding nearly equal energy losses for the same fragments of interest.

The primary beam intensity was monitored by the counting rate in a  $\text{BaF}_2$  detector located near the targets. The output of the  $\text{BaF}_2$  detector was normalized to the readings of a Faraday cup at the exit of the cyclotron. Fragments produced and emitted at very forward angles were transmitted and separated based on their mass-to-charge ratio ( $A/Q$ )

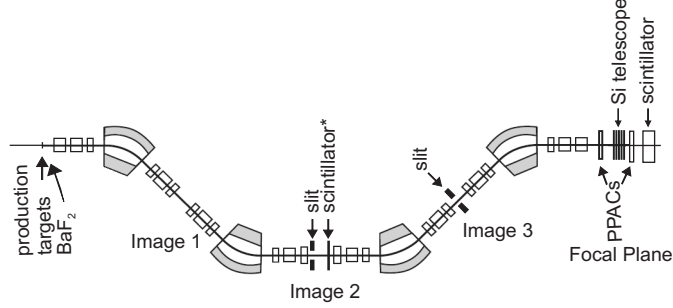


FIG. 1: Configuration of the A1900 used in the current work. Note that the Image2 scintillator was inserted only at the highest rigidity setting.

using the A1900 fragment separator [8]. Slits located at the Image2 and Image3 focal points were used to limit the momentum acceptance of the A1900 to  $\Delta p/p = \pm 0.5\%$  about the central beam axis, c.f. Fig. 1. The fragments were selected and transmitted through the separator by varying the magnetic rigidity ( $B\rho$ ) of the whole device from 3.628 to 5.228 Tm. The rigidities were chosen based on predicted maxima of the momentum distributions for the  $A = 22 - 31$  fluorine isotopes using the program LISE [9]. At the highest magnetic rigidity, the Image2 and Image3 slits were fully opened to an momentum acceptance of  $\Delta p/p = \pm 2.5\%$  in order to observe the production of nuclei along the neutron drip line. Five  $5 \times 5 \text{ cm}^2$  Si PIN detectors with thicknesses of 980, 966, 1001, 988, and 992  $\mu\text{m}$ , and a 10-cm thick plastic scintillator with an active area of  $15 \times 10 \text{ cm}^2$ , both located at the focal plane  $\sim 35 \text{ m}$  downstream from the target, were used to measure the energy losses and kinetic energies of the fragments in order to identify each transmitted particle. The 966- $\mu\text{m}$  thick Si PIN (#2) detector and the thick plastic scintillator were also used to provide start signals for the time-of-flight (*TOF*) relative to the cyclotron's radio frequency (*RF*) for the  $\sim 35 \text{ m}$  path length from the target to the focal plane. A pair of parallel plate avalanche counters (*PPAC*'s) located in the focal plane position was used to track the ions and to correct for different path lengths travelled by the particles. A thin 28-mg/cm<sup>2</sup> thick plastic scintillator positioned at the Image2 plane provided additional information on the trajectory of the ions measured at the largest rigidity setting ( $\Delta p/p = \pm 2.5\%$ ).

### III. RESULTS AND DISCUSSION

All of the data were treated on an event-by-event basis. The nuclear charge:

$$Z \propto m \sqrt{\frac{dE/dx}{\beta^2} (\log(\gamma^2) - \beta^2)} \quad (1)$$

and the mass-to-charge ratio:

$$\frac{A}{Q} \propto \frac{P}{Q\beta\gamma} \propto \frac{B\rho}{\beta\gamma}, \quad (2)$$

were calculated from the energy loss ( $dE/dx$ ) at each rigidity setting ( $B\rho$ ) using the Lorentz factor ( $\gamma$ ) and relativistic velocity ( $\beta$ ) deduced from the *TOF* in order to reconstruct the momentum distribution for each isotope in the lab frame. The positions of the fragments at the focal plane were also used to calculate their momenta/rigidities to resolve the isotopes at the largest angular acceptance of the separator ( $\Delta p/p = 5.0\%$ ). The resolution for  $A/Q$  and  $Z$  of  $\sim 0.5\%$  and  $1.0\%$  were achieved after applying the position correction to the rigidities, for example see Fig. 2. The measured fragment intensities at the achromatic focal plane were corrected for the angular transmission through the separator by using the convolution model in version 7.4.75 of the simulation program LISE++ [9, 10]. In this model, the angular transmissions were calculated with the assumption that the momentum distributions were Gaussian shaped with an exponential tail on the low momentum side.

The measured experimental fragment yields were fitted with an asymmetric Gaussian

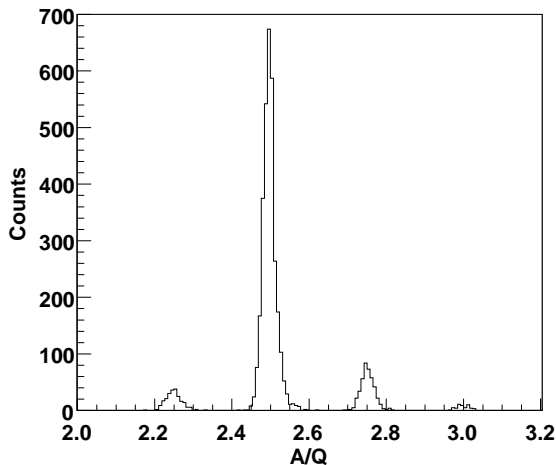


FIG. 2: The mass resolution of the fully striped beryllium isotopes produced by the fragmentation with the Ni target observed at the focal plane at a magnetic rigidity of 4.228 Tm.

of the form:

$$\frac{d\sigma_{\parallel}}{dp} = y_o \text{Exp}\left[\frac{-(x - x_o)^2}{2\sigma^2\left(1 + \frac{\delta a(x_o - x)}{\sqrt{2}\sigma}\right)}\right], \quad (3)$$

where  $y_o$  is a normalization factor and  $\delta a$  is related to the asymmetry factor  $a$  by:

$$\delta a = \begin{cases} 0 & x \geq x_o \\ a & x < x_o. \end{cases}$$

The results of the fitting procedure using Eq. 3 for the momentum distribution of  $^{25}\text{F}$  produced from the fragmentation of  $^{40}\text{Ar}$  with the tantalum target is shown in Fig. 3 with the parameters  $y_o = 7.3 \times 10^{-3}$ ,  $x_o = 11.99$ ,  $\sigma = 0.44$  and  $a=0.36$ .

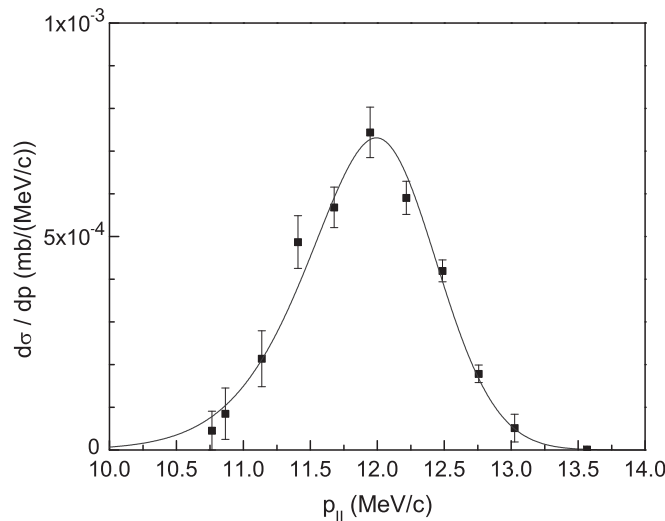


FIG. 3: The filled squares are the differential parallel momentum distributions of  $^{25}\text{F}$  measured at the A1900 focal plane. The curve represents the fit to the data using an asymmetric Gaussian function described in the text.

The resulting values of the centroid ( $x_o$ 's), widths ( $\sigma$ 's) and isotropic yields for each of the three targets used with the  $^{40}\text{Ar}$  projectile were obtained for all of the observed fragments and compared to an empirical model and several simulations. The systematic variations of the data are discussed below.

### A. Differential Energy Loss

The interaction of charged particles with matter results in a loss in all or part of the ion's kinetic energy due to ionization of the medium. In the present case, the change in the kinetic

energy of the fragments produced by projectile fragmentation passing through the remainder of the target results in a shift to lower energies and a broadening of the momentum distribution. Since the fragment can be produced at any point along the projectile's path through the target, a substantial spread may be created in the observed momentum distribution with a thick target. The deconvolution of the energy loss from the measured momenta is necessary in the present case with the thick targets to study the systematics of the reaction mechanism. The effect of the target thickness on the energy of the fragment ( $E_f$ ) produced from the fragmentation of the projectile with bombarding energy  $E_{bo}$  has been described in Ref. [11]. This method was used in the present work to correct for the mean energy loss through the targets and is briefly outline below.

The kinetic energy of a fragment created at a depth  $\delta$  in a given medium of thickness  $t$  may be expressed as:

$$E_f(\delta) = E_{bo} \left( 1 - \frac{\delta}{R_{bo}} - \frac{t - \delta}{R_{fo}} \right)^{-\xi}, \quad (4)$$

where  $R_{bo}$  and  $R_{fo}$  are the projectile and fragment ranges for a given initial energy  $E_{bo}$ , respectively. The range of an ion with  ${}^AZ$  can be parameterized by three constants,  $k$ ,  $\xi$  and  $C$ , which depend on the stopping material such that:

$$R = k \frac{A}{Z^2} \left( \frac{E}{A} \right)^\xi + CA. \quad (5)$$

The constants  $k$ ,  $\xi$ , and  $C$  for the targets used in the current work were determined from fitting this function to the particle ranges in Ref. [12]. Thus, with the aid of Eq. 5, the energy and velocity of the fragment at the center of the target and the momentum broadening due to the energy loss can be calculated as discussed in the next section.

## B. Parallel Momentum Width

As indicated above, the measured variance of the longitudinal momentum distribution ( $\sigma_{tot}$ ) will be a convolution of the nuclear reaction and the differential stopping of the ion. Thus, the measured variance due to the slowing of particles is related to the momentum dispersion  $\sigma$  via the equation [11]:

$$\sigma_{tot}^2 \simeq \frac{(E_f(\delta = t) - E_f(\delta = 0) + \Delta E_N (1 - (1 - \frac{t}{R_{fo}})^{1/\gamma-1})^2)}{4} + \frac{|\sigma_N(\sigma, E_f(\delta = t)) - \sigma_N(\sigma, E_b)|^2}{4}. \quad (6)$$

The first term in Eq. 6 is due to the energy spreading of the fragment through the thickness of the target and is proportional to the difference in the fragment cutoff energies ( $E_f(\delta = t), E_f(\delta = 0)$ ) and a corrective term  $\Delta E_N$  that is related to the energy loss of the fragments through remainder of the target (calculated via the derivative of Eq. 4 with the range of the projectile equal to zero). The second term is due to the energy straggling of the particles, projectile and fragment, through the remainder of the target. The momentum dispersion term  $\sigma$  is related to  $\sigma_N$  by:

$$\sigma_N(\sigma, E_i) = 2\sigma \frac{E_i}{p_i} \left(1 - \frac{t - \delta}{R_{fo}}\right)^{1/\gamma-1} \quad (7)$$

where  $E_i$  and  $p_i$  are the kinetic energy and momentum of the fragment created at the end back of the target ( $\delta = t$ ) or the kinetic energy and momentum of the projectile ( $\delta = 0$ ).

Using Eqs. 4 through 7, the momentum dispersion term can be solved for and calculated for each fragment. The correction factors for the parallel momentum distribution due to the energy straggling of the fragments were found to vary from 25-60%. The corrected parallel momentum widths obtained for the nuclear reaction are shown in Fig. 4 as a function of total mass loss by the projectile. The widths were obtained by fitting the momentum distributions to Eq. 3 after correcting the measured variances in the projectile frame for the differential energy loss with Eq. 6. As mentioned above, the shapes of distributions give hints into the reaction process. The fragments are expected to have Gaussian momentum distributions due to the statistical processes that create the fragments in the fast disintegration process. From the conservation of momentum in the rest frame of the projectile, it has been shown that an emission of a random cluster of  $\Delta A$  nucleons from a  ${}^A Z$  projectile would lead to a parallel momentum width proportional to the square root of the product of the mass loss times the ratio of the number of nucleons in the fragment to the number of nucleons in the projectile minus one, the so-called Goldhaber expression[13]. If during the fragmentation process, the nucleons were emitted over the total interaction time through sequential evaporation instead of in a single cluster, the parallel momentum width may be approximated by the square root of the mass difference times a constant known as the reduced width [14]. The key difference between the two results is the latter, for sequential emission, continues to grow with mass loss as shown in Fig. 4 by the dotted curves. The predicted momentum widths from the sequential emission model using a reduced width of 85 MeV/c only agrees with the calculated widths for projectile-like fragments that lose less than half the mass of the projectile. Instead

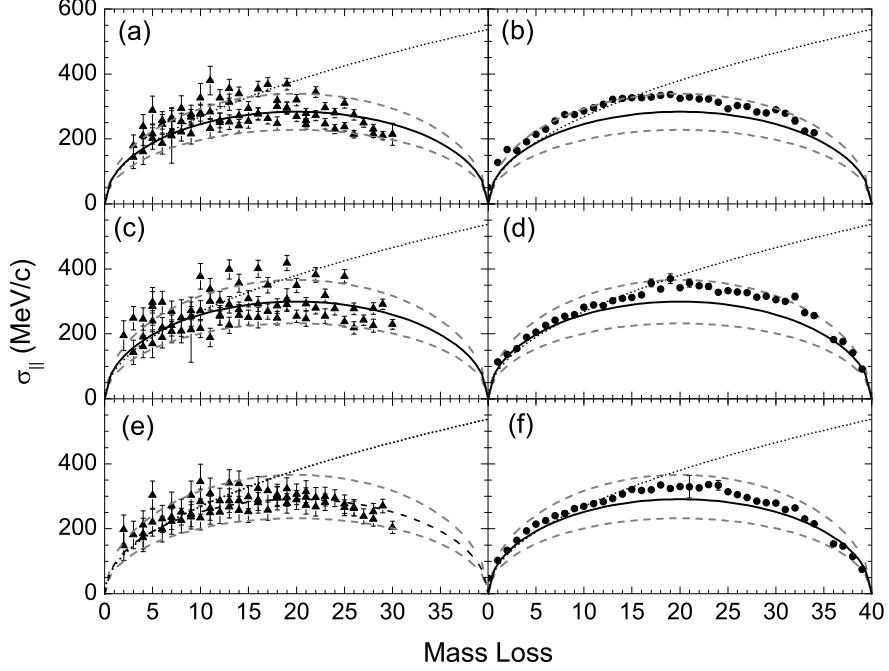


FIG. 4: The parallel widths of nuclei produced in the reaction of (a)  $^{40}\text{Ar}+^9\text{Be}$ , (c)  $^{40}\text{Ar}+^{\text{nat}}\text{Ni}$  and (e)  $^{40}\text{Ar}+^{181}\text{Ta}$ . The solid and dotted curves are the line shapes predicted by a single cluster [13] and sequential emission of nucleons [14] during the interaction of the projectile and target. The filled circles in the panels b, d, and f are the calculated widths from the ISABEL-GEMINI code [6, 15] compared to the single cluster and sequential emission of nucleons model from panels a, c and e respectively.

the measured widths from the fragmentation of  $^{40}\text{Ar}$  with Be, Ni, and Ta from the current work and the calculated widths appear to follow the shape predicted by the former model assuming a single emission of a cluster of nucleons. The parallel momentum widths obtained from the reactions with the Ta, Ni, and Be targets were fitted to the function from the single emission of particles and reduced widths of 85(15), 85(20), and 86(13) MeV/c were obtained for the fragmentation on the Be, Ni, and Ta targets, respectively. The dashed curves shown in Fig. 4 represent one standard deviation uncertainties in the fitted values. The large variances are most likely due to the overestimation (underestimation) of the energy loss through the thick targets used in the current experiment for the heaviest (lightest) isotope in an elemental chain. The reduced widths from calculations with the ISABEL-GEMINI

code for the reactions in the Be, Ni and Ta targets, shown by the open circles for the in Fig. 4(a), (b), and (c), respectively, were found to be slightly larger but approximately within one sigma of the values found in the current work. The values of the reduced widths also agree with published values ( $\sigma_o \sim 90$  MeV/c) from fragmentation of projectiles with bombarding energies greater than 80 MeV/nucleon (see Refs. [16, 17]), suggesting that the momenta produced by the fragmentation mechanism is independent of the target/projectile combination.

### C. Parallel Momentum Transfer

The interactions during the collision between the projectile and target nuclei also can alter the mean nuclear velocities of the prefragments. This change in the velocity comes naturally from the removal of bound nucleons and has also been attributed to a friction phenomenon [18]. The net momentum transfer to the average perpendicular momentum

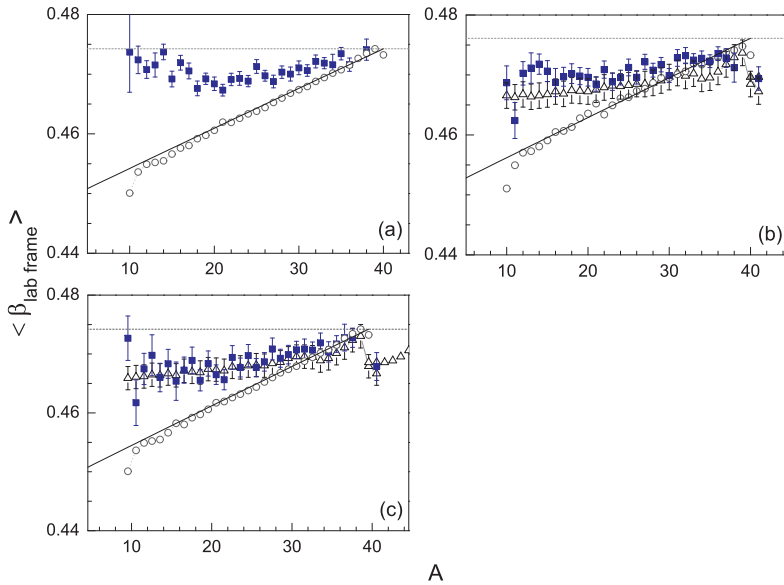


FIG. 5: (Color Online) A comparison of the measured average isobaric velocities from the current work, filled squares, with the predicted velocities of the projectile fragments from ISABEL-GEMINI and DIT-GEMINI, unfilled circles and triangles, respectively. The horizontal dashed lines are the projectile's velocity in the lab frame and the solid curves are the velocity of the fragments using Eq. 8. Panels (a)-(c) represent the same reactions as those in Fig. 4.

component is not observable in the present work due to the equal probabilities of the projectile interacting on either side of the target nucleus [19], while the longitudinal momentum lost in the projectile's rest frame by the participant nucleons during the collision has been found to be related to the average fragment velocity ( $\langle \beta_{\parallel} \rangle$ ) by the expression:

$$- \langle P'_{\parallel} \rangle = m_t \langle \beta_{\parallel} \rangle \frac{\beta\gamma}{\gamma + 1}, \quad (8)$$

where  $m_t$  is the mass of the target and  $\gamma$  is the Lorentz factor [14]. For target fragmentation, the momentum transfer per nucleon lost by the target was found empirically to be roughly a constant equal to the average binding energy per nucleon in heavy nuclei, 8 MeV/c/nucleon, and this systematic behavior has been observed in many projectile fragmentation reactions.

The average parallel momentum transfers observed in the current work are shown in panels (a), (b) and (c) of Fig. 5 after correcting for the differential energy loss for the fragmentation of  $^{40}\text{Ar}$  with Be, Ni, and Ta, respectively. The isotopic velocities were calculated from the sum of the fragment velocities which were weighted by their respective measured cross sections divided by the sum of the of the isobar cross section (*i.e.* the fragmentation probability for a given isotope). Comparison with the observed values with predictions of the momentum transfer to the participant nuclei from the projectile from the DIT and ISABEL codes are also shown in Fig. 5. No calculations were done using the DIT code for the reaction of  $^{40}\text{Ar}$  with Be due to the fact that the small target size that could not be accommodated by the code. The resulting intermediate fragments from both codes were used as input to the GEMINI code [15] in order to statistically deexcitate the prefragment distributions. A linear increase in the velocities was found with mass loss for the residues from calculations using ISABEL-GEMINI. The slopes were found to be similar to those predicted Morrissey [14] but this linear trend does not agree with the measured results for large mass loss. Instead, the velocities of the light fragments follow the behavior predicted by the DIT-GEMINI calculations. This so-called reacceleration behavior for large mass loss has also been observed in fragmentation at significantly higher energies around 1 GeV/nucleon [20, 21] and is thought to be due to momentum transfers from the participant blast during the interaction with the participant nucleons with the spectator nucleons [22]. This surprising agreement with the DIT-GEMINI calculations suggest that the deep inelastic transfer process may persist in reactions that occur at intermediate projectile energies of  $\sim 120$  MeV/nucleon as suggested by Ref. [7].

## D. Cross Sections

The isotropic yields of fragments from projectile fragmentation were determined by numerical integration of Eq. 3 for each isotope and converted to reaction cross sections. Sta-

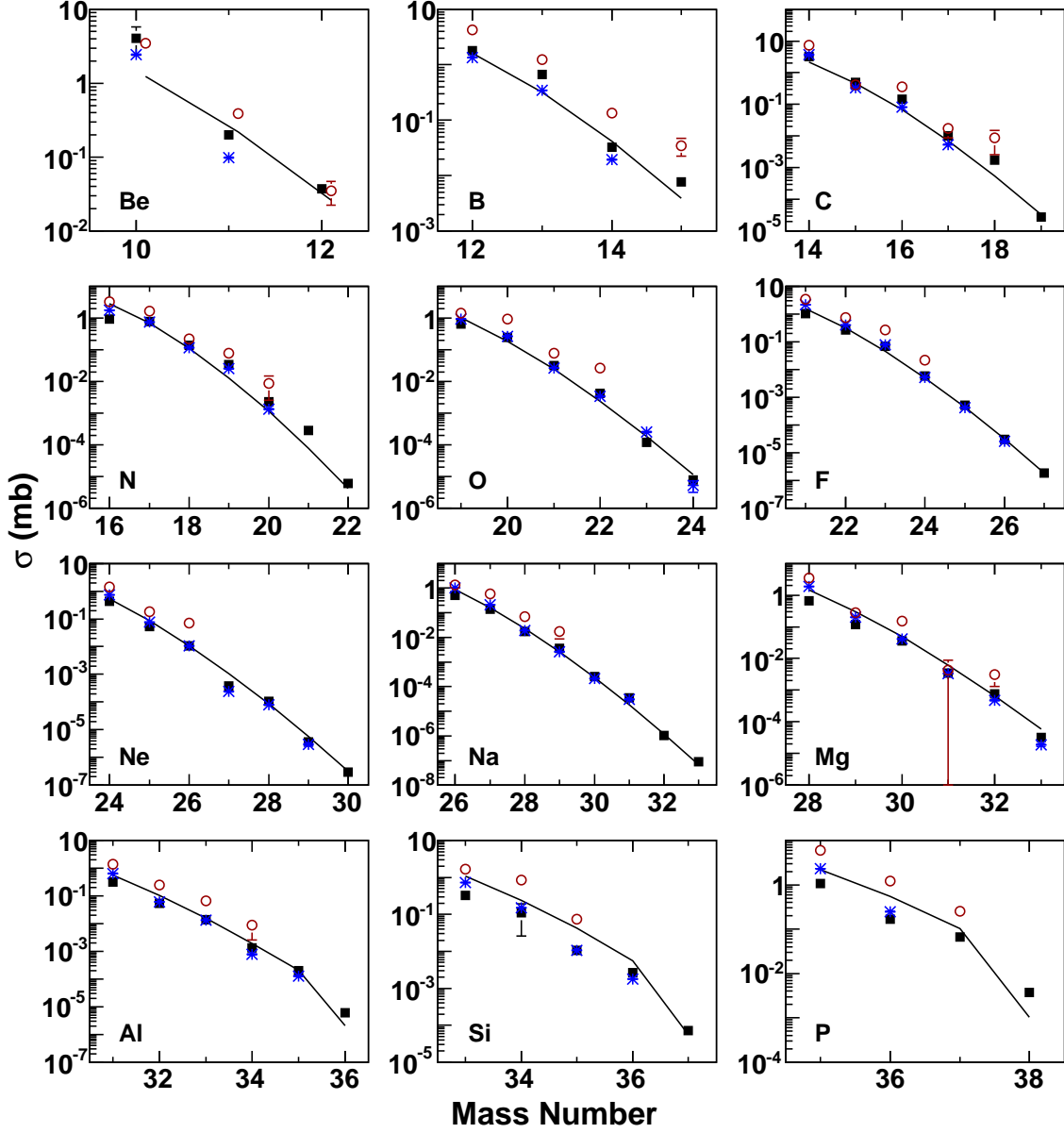


FIG. 6: (Color Online) Comparisons of the cross sections for the neutron-rich beryllium to phosphorus isotopes produced in the reaction of  $^{40}\text{Ar}$  with  $^9\text{Be}$  from the current work and with previous data taken at RIKEN [23], filled squares and stars, respectively. Also shown are the predictions by the empirical formula EPAX (solid line) and simulations from ISABEL-GEMINI (open circles).

tistical errors were calculated by numerical integration using the Leibniz theorem similar to the method outlined in Ref. [24]. The resulting cross sections from the reaction of  $^{40}\text{Ar}$  with Be, Ni, and Ta for fragments with  $Z = 4$  to 15 are shown by the filled squares in Figs. 6, 7 and 8, respectively. The cross sections from the fragmentation of  $^{40}\text{Ar}$  rising thin targets of

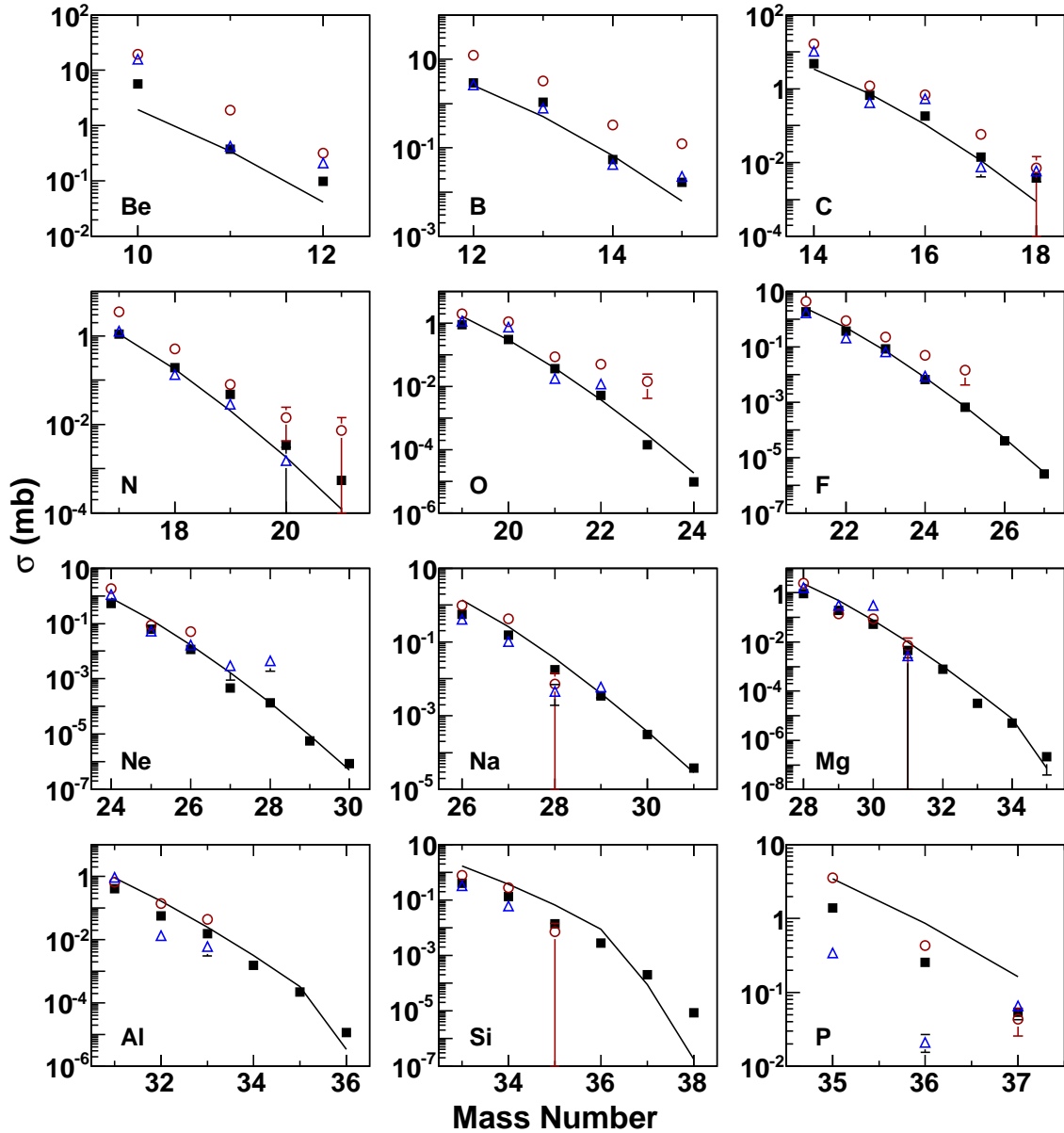


FIG. 7: (Color Online) The cross sections of the neutron-rich beryllium to phosphorus isotopes produced in the reaction of  $^{40}\text{Ar}$  with  $^{nat}\text{Ni}$ . The cross sections from the current work, square, are compared with predictions by EPAX, solid line, and simulations by ISABEL-GEMINI and DIT-GEMINI, open circles and triangles, respectively.

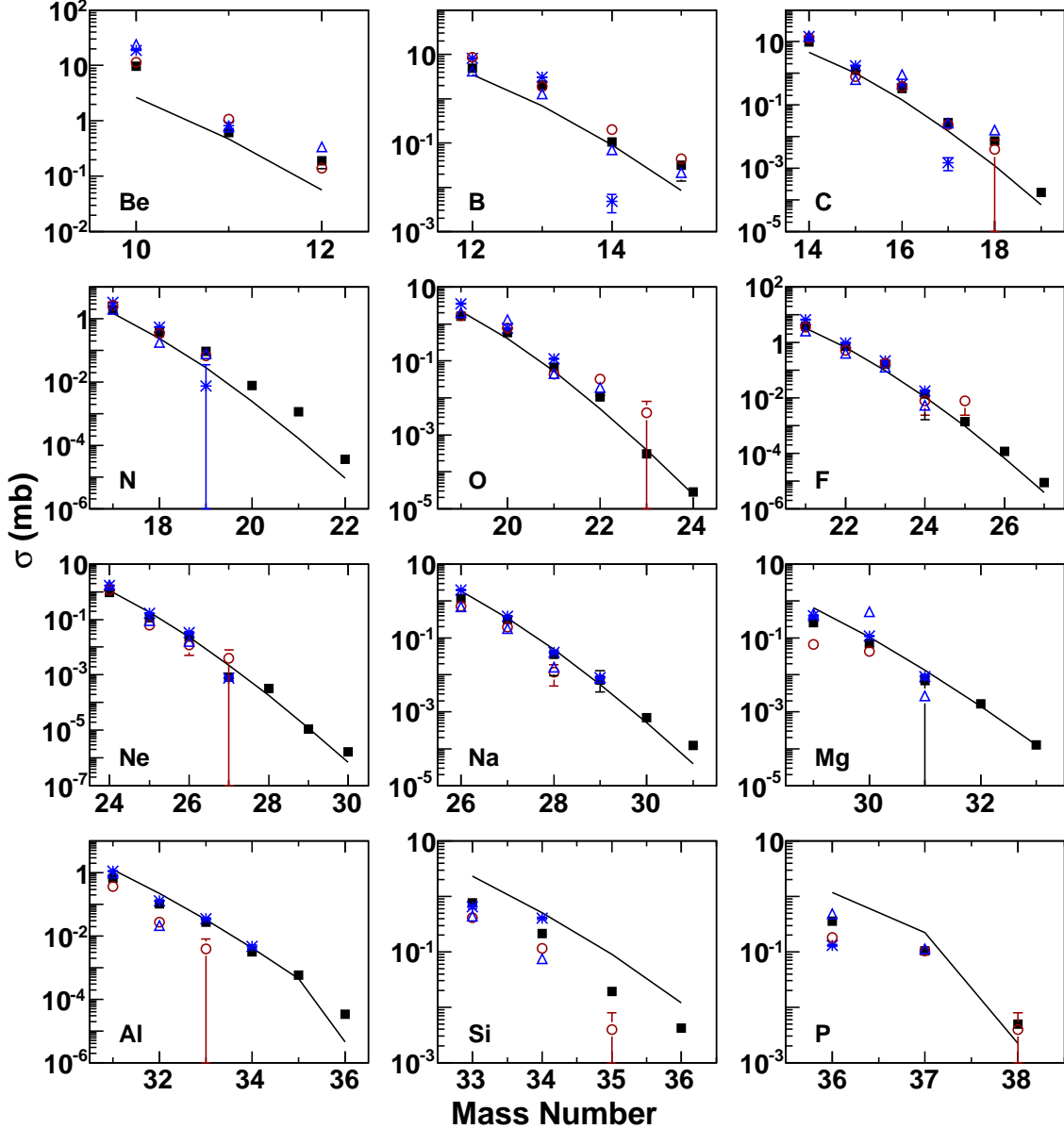


FIG. 8: (Color Online) The cross sections of the neutron-rich beryllium to phosphorus isotopes produced in the reaction of  $^{40}\text{Ar}$  with  $^{181}\text{Ta}$ . The symbols retain their meaning from Figs. 6 and 7.

Be and Ta previously obtained by Notani *et al.* [23] as stars at 90-94 MeV/nucleon are displayed, predictions from EPAX are drawn as curves and the results from calculations using ISABEL-GEMINI and DIT-GEMINI as the unfilled symbols are also included for comparison. In all cases, exponential decreases in the reaction cross sections with mass number for all isotopes are observed or predicted. As mentioned in Section III D, it is expected that

in the regime of “limiting fragmentation” the cross sections are expected to be independent of bombarding energy, thus we expect to obtain similar cross sections to those in Ref. [23]. The values published by Notani *et al.* for fragmentation with the Be and Ta targets and from the results of the DIT-GEMINI code for the reaction with Ni and Ta targets for agree with the current work to within a factor of two. The predictions for the fragmentation cross sections from EPAX are also within a factor of two for isotopes lighter than the mass of the projectile. Note that it was previously observed that EPAX systematically over predicted the yields for products with  $A > 25$  in the Ar + Be reaction [23]. The ISABEL-GEMINI code also over predicted the cross sections for the reaction of  $^{40}\text{Ar}$  with the Be and Ni targets by as much as a factor of five yet generally agrees with the cross sections obtained for the  $^{40}\text{Ar} + \text{Ta}$  reaction.

The effect of the target neutron excess on the  $N/Z$  of the fragments can be investigated by a comparison of the fragment cross sections from each of the three different  $N/Z$  targets. Shown in the left and right panels of Fig. 9 are the ratios of the cross sections of the fragments produced in the reactions of  $^{40}\text{Ar}$  with the Ni and Ta targets to the same fragments produced in the Be target, respectively. The data are shown as a function of the neutron excess beyond the  $N/Z$  ratio of the most neutron-rich isotope in the line of stability. The cross sections were further normalized by a geometric target-projectile collision cross section defined by Bradt and Peters [25] as:

$$\sigma_t^{geo} = \pi r_o^2 (A_t^{1/3} + A_p^{1/3} - r_b)^2, \quad (9)$$

where  $A_t$  and  $A_p$  are the atomic masses of the target and projectile, respectively. The overlap parameter ( $r_b$ ) is an energy-independent parameter whose value can vary, see for example Refs. [26, 27]. In the present work, the values of  $r_o = 1.35$  fm and  $b = 0.83$  were adopted based on the work of Ref. [28] for the fragmentation of 1.88 GeV/nucleon  $^{56}\text{Fe}$  by various targets.

If the yields do not depend on the target then the ratio of the normalized cross sections are expected to be independent of the neutron excess. In the left panel of Fig. 9, one can see that almost no enhancement is observed for fragmentation with the Ni target but an enhancement of a factor of two can be seen for the largest  $N/Z$  isotopes produced in the fragmentation with a tantalum target (right panel). The nuclei with enhanced cross sections correspond to the most neutron-rich isotopes closest to the neutron drip line. This enhancement for nuclei with large neutron excess may become important in the search for

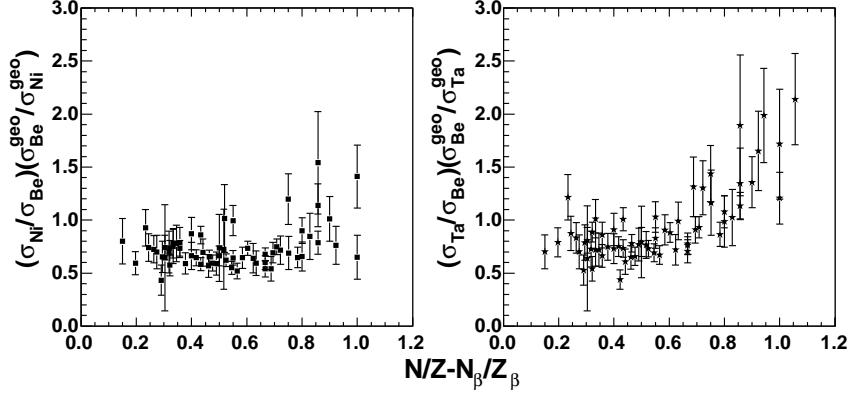


FIG. 9: The ratio of the cross sections of neutron rich fragments produced in the reactions of  $^{40}\text{Ar}$  with  $^{nat}\text{Ni}$  and  $^{181}\text{Ta}$ , left and right panels, respectively, relative to those produced from the fragmentation of  $^{40}\text{Ar}$  with  $^9\text{Be}$  are shown as a function of the excess neutron-to-proton ratio. The neutron-to-proton ratio is relative to the largest neutron-to-proton ratio of the beta stability isotope for each element. See text for explanation of the normalization factor.

the location of the neutron drip line and should be taken into account in future empirical parameterizations of the production cross sections. We also note that the average values of the ratios are less than one so the average cross sections in the present work are lower than the expected ratios from the higher energy work of Ref [28].

#### IV. SUMMARY

In the present work, the neutron-rich reaction products from the projectile fragmentation of a  $\sim 120$  MeV/nucleon  $^{40}\text{Ar}$  beam in beryllium, nickel and tantalum were investigated at the NSCL using the A1900 fragment separator. An asymmetric Gaussian was found to describe the momentum distributions. Two hundred and one momentum distributions were fitted with a momentum distribution function to extract the parallel momentum transfer, parallel momentum width, and fragmentation cross section. Comparisons with the predictions from an internuclear cascade code ISABEL and a deep inelastic transfer code DIT, where both codes were coupled to a statistical deexcitation code GEMINI, were made in an attempt to understand the reaction mechanism. The parallel momentum transfer calculated by the ISABEL-GEMINI code was found to follow the linear trend with the same slope predicted by previous systematics, but only qualitatively agrees with the observed values for small

mass losses. Instead, the parallel momentum transfer was observed to increase in velocity for large mass losses similar to the behavior patterns predicted by the DIT-GEMINI code. This reacceleration effect has been previously ascribed to arise due to the interaction of the non-participating or spectator nucleons with the participant blast.

The measured parallel momentum widths were observed to have a parabolic dependence on the mass loss from the projectile for all projectile/target combinations. This shape was predicted by the statistical emission of a single fragment during the interaction and by the Monte Carlo code ISABEL-GEMINI. The reduced widths from the present work were found to be  $\sim 85$  MeV/c and independent of the target and projectile combination. These values agree with published literature values for higher bombarding energies and the values predicted by ISABEL-GEMINI are within one sigma of the current work. The reaction cross sections were measured for 201 momentum distributions and compared with the DIT-GEMINI, ISABEL-GEMINI codes and the empirical parameterization formula EPAX. Fairly good agreement was found between the cross sections obtained by EPAX and previous measurements from Ref. [23] using thin targets and also with the predictions from the calculations from DIT-GEMINI and ISABEL-GEMINI. Finally, a large enhancement was found for the most neutron-rich nuclei in a comparison of the fragmentation yields from the Ta and the Be targets suggesting that the neutron excess of the target does have an effect on the reaction at intermediate energies.

### Acknowledgments

The authors would like to thank G. A. Souliotis for his assistance with the DIT-GEMINI simulations. This work was supported in part by the National Science Foundation under the grant PHY-01-01523 and performed under the auspices of the U.S. Department of Energy by Lawrence Livermore National Laboratory under Contract DE-AC52-07NA27344.

- 
- [1] M. Theoennessen, Rep. Prog. Phys **67**, 1187 (2004).
  - [2] K. Sümmerer and B. Blank, Phys. Rev. C **61**, 034607 (2000).
  - [3] T. R. Werner et al., Z. Phys. **A358**, 169 (1997).
  - [4] D. Guerreau, Nucl. Phys. A **447**, 37 (1985).

- [5] K. Chen et al., Phys. Rev. **166**, 949 (1968).
- [6] Y. Yariv and Z. Fraenkel, Phys. Rev. C **24**, 488 (1981).
- [7] L. Tassan-Got and C. Stépan, Nucl. Phys. A **524**, 121 (1991).
- [8] D. J. Morrissey et al., Nucl. Instr. and Meth. B **2003**, 90 (2003).
- [9] O. Tarasov and D. Bazin and M. Lewitowicz and O. Sorlin, Nucl. Phys. A **701**, 661 (2002).
- [10] O. Tarasov, Nucl. Phys. A **734**, 536 (2004).
- [11] J. Dufour et al., Nucl. Instr. and Meth. A **248**, 267 (1986).
- [12] F. Hubert, R. Bimbot, and H. Gauvin., At. Data and Nucl. Data Tables **60**, 61 (1990).
- [13] A. Goldhaber, Phys. Lett. B. **53**, 306 (1974).
- [14] D. Morrissey, Phys. Rev. C **39**, 460 (1989).
- [15] R. Charity, Nucl. Phys. A **483**, 391 (1988).
- [16] D. Greiner et al., Phys. Rev. Lett **35**, 152 (1975).
- [17] G. Farés et al., Eur. Phys. J. A **19**, 105 (2002).
- [18] J. H. A. Abul-magd and B. Schürmann, Phys. Lett. B **60**, 327 (1976).
- [19] K. V. Bibber et al., Phys. Rev. Lett **43**, 840 (1979).
- [20] T. Enqvist et al., Nucl. Phys. A **658**, 47 (1999).
- [21] M. V. Ricciardi et al., Phys. Rev. C **73**, 041607 (2006).
- [22] L. Shi, P. Danielewicz, and R. Lacey, Phys. Rev. C **64**, 043601 (2001).
- [23] M. Notani et al., Phys. Rev. C **76**, 044605 (2007).
- [24] *Genie 2000 Customization Tools Manual* (2000).
- [25] H. Bradt and B. Peters, Phys. Rev. **77**, 54 (1950).
- [26] L. W. Townsend and J. W. Wilson, Radiat. Res. **106**, 284 (1986).
- [27] W. R. Binns et al., Phys. Rev. C **36**, 1870 (1987).
- [28] G. D. Westfall et al., Phys. Rev. C **19**, 1309 (1979).